

# Electrical and Thermal Transport at the Planckian Bound of Dissipation in the Hydrodynamic Electron Fluid of $WP_2$

J. Gooth<sup>1\*</sup>, F. Menges<sup>1</sup>, C. Shekhar<sup>2</sup>, V. Süß<sup>2</sup>, N. Kumar<sup>2</sup>, Y. Sun<sup>2</sup>, U. Drechsler<sup>1</sup>, R. Zierold<sup>3</sup>, C. Felser<sup>2</sup>, B. Gotsmann<sup>1\*</sup>

<sup>1</sup>IBM Research -Zurich, Säumerstrasse 4, 8803 Rüschlikon, Switzerland.

<sup>2</sup>Max Planck Institute for Chemical Physics of Solids, Nöthnitzer Straße 40, 01187 Dresden, Germany.

<sup>3</sup>Institute of Nanostructure and Solid-State Physics, Universität Hamburg, Jungiusstraße 11, 20355 Hamburg, Germany

\*johannes.gooth@outlook.com, bgo@zurich.ibm.com

## Abstract:

Materials with strongly-correlated electrons exhibit interesting phenomena such as metal-insulator transitions and high-temperature superconductivity. In stark contrast to ordinary metals, electron transport in these materials is thought to resemble the flow of viscous fluids. Despite their differences, it is predicted that transport in both, conventional and correlated materials, is fundamentally limited by the uncertainty principle applied to energy dissipation.

Here we discover hydrodynamic electron flow in the Weyl-semimetal tungsten phosphide ( $WP_2$ ). Using thermal and magneto-electric transport experiments, we observe the transition from a conventional metallic state, at higher temperatures, to a hydrodynamic electron fluid below 20 K. The hydrodynamic regime is characterized by a viscosity-induced dependence of the electrical resistivity on the square of the channel width, and by the observation of a strong violation of the Wiedemann-Franz law. From magneto-hydrodynamic experiments and complementary Hall measurements, the relaxation times for momentum and thermal energy dissipating processes are extracted. Following the uncertainty principle, both are limited by the Planckian bound of dissipation, independent of the underlying transport regime.

## Main Text:

In an overwhelmingly large group of conducting materials, charge transport can be described by the rather simple model of a free-electron gas. The base of which is that the carriers move unimpededly until they scatter with phonons or defects. Such collisions relax both, the momentum and the energy, and consequently impose a resistance to charge and heat flow alike. In most conventional conductors, electrical and thermal transport are therefore related *via* the Wiedemann-Franz law, which states that the product of the electrical resistivity  $\rho$  and the thermal conductivity  $\kappa$ , divided by the temperature  $T$  is a constant  $L = \rho\kappa/T$ , usually yielding the Sommerfeld value  $L_0 = 2.44 \times 10^{-8} \text{ W}\Omega\text{K}^{-2}$ .  $\rho$  and  $\kappa$  are intrinsic material properties, independent of the size and geometry of the conducting bulk. The conventional free-electron model, however, fails to describe transport in strongly-interacting electron systems (1). The difficulty is to find a theoretical framework capturing the frequent inter-particle collisions that define the interaction within the many-electron system. Recently, it has been suggested that the theory of hydrodynamics, which is normally applied to explain the behavior of classical liquids like water, could be employed to describe the collective motion of electrons in such a system (1–5).

In contrast to the free-electron gas, the energy dissipation in a hydrodynamic electron fluid is defined by momentum-conserving electron-electron scattering. Consequently, the electrical resistance of a hydrodynamic electron liquid is proportional to its shear viscosity and therefore paradoxically increases with increasing mean free path of the electrons (2, 6). Another signature of the hydrodynamic nature of transport emerges when the flow of the electrons is restricted to channels (7, 8). Viscosity-induced shear forces at the channel walls cause a non-uniform velocity profile, making the electrical resistivity a function of the channel width. Moreover, the electrical resistivity will tend to zero, because momentum-relaxing processes are strongly suppressed. As the thermal conductivity, however, is always finite, a strong violation of the Wiedemann-Franz law is predicted (1, 3, 4, 9).

Despite the significant difference in the microscopic mechanisms behind momentum- and energy-relaxing collisions, it has recently been proposed that, in both processes, dissipation is tied to a universal upper bound of entropy production with a time scale of  $\tau_{\hbar} = \hbar/(k_B T)$  (1, 10).  $\tau_{\hbar}$  is set only by the Boltzmann constant  $k_B$ , the reduced Planck constant  $\hbar$  and the temperature  $T$ . This concept of “Planckian dissipation” has been developed within the framework of the uncertainty principle (1) and a string theory, known as anti-de-Sitter space/conformal field theory correspondence (AdS/CFT) (11–15). Holographic models successfully predicted the universal bound on the momentum-relaxation time  $\tau_{\text{mr}}$  in a strongly interacting neutral plasma (16). The momentum-relaxation bound  $\tau_{\text{mr}} \geq \tau_{\hbar}$  can also be expressed as the ratio of the shear viscosity to the entropy density and is not only supported by experiments on the quark-gluon plasma and on the ultra-cold Fermi gas (17, 18), but is also well-respected in classical fluids such as water.

Likewise, maximally dissipative processes, matching the timescale  $\tau_{\hbar}$  have recently been proposed to underpin the  $T$ -proportional resistivity of metals (1, 10), and are believed to be at the root of high-temperature superconductivity (12, 19). In the context of charge transport described by quasi-particles,  $\tau_{\text{md}}$  represents the characteristic scattering time to randomize the excess forward momentum of a quasi-particle. Momentum relaxation in most conductors is determined by the way in which the electrons couple to the lattice or the disorder of the host solid. Thus,  $\tau_{\text{mr}}$  of the electron system is determined by extrinsic coupling parameters and is not generally universal (1). In the hydrodynamic regime, the momentum and thermal energy relaxation are independent processes,

which in principle enables the isolation of the intrinsic relaxation time  $\tau_{\text{er}}$ .  $\tau_{\text{er}}$  represents the characteristic time to dissipate the excess thermal energy of a quasi-particle. Indeed, hydrodynamic effects have been postulated to play a role in the  $T$ -linear resistivity of high-temperature superconductors above their critical temperature, but purely hydrodynamic transport is not directly applicable to most of those systems. Extracting  $\tau_{\text{mr}}$  and  $\tau_{\text{er}}$  separately from experimental data has remained challenging, because of the strong momentum-relaxation contribution. In fact, as momentum-relaxation processes are always present in a real material system, momentum can only be quasi-conserved. This, however, does not mean that hydrodynamic signatures are not observable in transport experiments. Hydrodynamic effects become dominant, when electron-electron scattering provides the smallest spatial scale in the system  $l_{\text{er}} \ll w \ll l_{\text{mr}}$ , where  $l_{\text{er}} = v_{\text{F}}\tau_{\text{er}}$  is the electron-electron scattering length,  $w$  the sample width,  $l_{\text{mr}} = v_{\text{F}}\tau_{\text{mr}}$  the mean free path and  $v_{\text{F}}$  the Fermi velocity (7, 20).

Inspired by pioneering experiments on semiconductor wires (21), signatures for hydrodynamic electron flow were recently reported in ultraclean PdCoO<sub>2</sub> (20) and graphene (22–24). However, as these materials exhibit only relatively weak-scattering, experimental evidence of a universal thermal dissipation bound has been elusive. It is therefore desirable to go beyond previous experiments and investigate the dissipative timescales of a strongly-correlated material in the limit of pure hydrodynamics.

For our study, we have chosen the semimetal WP<sub>2</sub> (25), because in this material momentum-relaxing scattering is anomalously strongly suppressed. WP<sub>2</sub> is a material with a space-group symmetry as the two-dimensional WTe<sub>2</sub>. It exhibits two pairs of two-fold degenerated Weyl points close to the intrinsic Fermi level. WP<sub>2</sub> contains a mirror plane perpendicular to the  $a$ -axis, a  $c$ -glide perpendicular to the  $b$ -axis and a two-fold screw axis along the  $c$ -axis. Owing to the high crystalline anisotropy, typical WP<sub>2</sub> crystals are needle-shaped with an orientation along the  $a$ -axis. Moreover, the magneto-transport in bulk single crystals has been shown to be highly anisotropic by 2.5 orders of magnitudes between the  $a$ - $c$  and  $a$ - $b$  plane, similar to bulk PdCoO<sub>2</sub> (26). Best single crystalline bulk samples of WP<sub>2</sub> exhibit a  $T$ -linear electrical resistivity above 150 K that is dominated by electron-phonon scattering and a temperature-independent resistivity below 20 K as previously observed in PdCoO<sub>2</sub> (20). Its residual resistivity is only 3 nΩcm, i.e. a remarkable three-times lower value than that of PdCoO<sub>2</sub> in the hydrodynamic regime. At temperatures between 20 and 150 K,  $\rho$  increases exponentially with increasing  $T$ , which has been attributed to the phonon drag effect. Phonon drag is considered beneficial for reaching the hydrodynamic regime, because it provides another source of momentum-conserving scattering (20). At 4 K, the bulk samples exhibit a mean free path of  $l_{\text{mr}} \approx 100 \mu\text{m}$  in the  $a$ - $c$  direction (Supplementary Material). The  $l_{\text{mr}}$  of WP<sub>2</sub> exceeds the momentum-relaxing scattering length of hydrodynamic PdCoO<sub>2</sub> and that of graphene (22, 23) by one and two orders of magnitude, respectively. These properties make WP<sub>2</sub> an ideal material for investigating hydrodynamic effects and the associated dissipative bounds in its strongly-correlated electron system.

For our experiments, we produced a series of WP<sub>2</sub> micro-ribbon by milling flux-grown single crystals. The high anisotropy of the crystal results in rectangular micro-samples that retain the needle-shaped orientation of the growth-crystal. Using a micro-manipulator, the milled micro-ribbons were transferred to a pre-defined metallic line structure (Fig. 1A). The solely mechanical fabrication method prevented chemical contamination and damage of the ultra-pure source material. Electron-beam deposition of platinum was used to provide electrical contacts by connecting the ribbon ends to the underlying metal lines. Electron microscopy was used to

determine the distance between the contact lines, i.e., the length  $l$  of the micro-ribbon along the  $a$ -axis of the crystal, its thickness  $t$  along the  $b$ -axis, and its width  $w$  along the  $c$ -axis. The transport direction in our samples matches the crystal's  $a$ -axis. The thickness is approximately  $t = w/2$ . However, the high anisotropy of the magneto-transport yields to a mean free path in  $a$ - $b$  direction of about 250-times lower than that in  $a$ - $c$  direction (26). Therefore,  $w$  is the characteristic length scale of the samples (25), justifying the use of two-dimensional models for the in-plane transport properties in  $a$ - $c$ . We investigated four with widths of 0.4  $\mu\text{m}$ , 2.5  $\mu\text{m}$ , 5.6  $\mu\text{m}$  and 9.0  $\mu\text{m}$ , all satisfying  $w \ll l_{\text{mr}}$  at low temperatures.

In a first set of transport experiments, we studied the  $T$  and  $w$ -dependence of the electrical resistivity  $\rho = V/I \cdot wt/l$  of the micro-ribbon (Fig. 1B). For this purpose, we measured the voltage response  $V$  to an AC-current bias  $I$ , using the standard low-frequency lock-in technique (Supplementary Materials). The elongated geometry of the micro-ribbons with contact lines across the full width of the samples was chosen to ensure to provide homogenous current distributions. Due to the low resistivity of the bulk sample, special care must be taken in extracting the intrinsic  $\rho$  of the  $\text{WP}_2$  ribbons. The quasi-four terminal resistivity measurements exclude the resistance of the contact lines, but in principle include the interface resistances at the metal/semimetal junction. The contact resistances are, however, negligible small, by means of not measurable, in comparison with real four-terminal measurements (Fig. S1). Conventionally,  $\rho = \rho_0 = m^*/(e^2 n \tau_{\text{mr}})$  is an intrinsic bulk property and does not depend on  $w$ . According to the Drude model,  $\rho$  only depends on the effective mass  $m^*$  of the charge carriers, the elementary charge  $e$  and the carrier concentration  $n$ . However, when boundary scattering becomes significant,  $\rho$  can turn into a function of the sample size (24). In in the well-established ballistic regime ( $w \ll l_{\text{er}}, l_{\text{mr}}$ ), for example, the electrical resistivity is given by  $\rho \sim w^{-1}$ . Further, in a purely hydrodynamic fluid ( $l_{\text{er}} \ll w \ll l_{\text{mr}}$ ), the flow resistance is solely determined by the interaction with the sample boundaries, reducing the average flow velocity of the electron fluid (Fig. 1C). Recent theory predicts that the electrical resistivity in the Navier-Stokes flow limit is modified as  $\rho = m^*/(e^2 n) \cdot 12 \eta w^{-2}$ , where electron-electron scattering is parameterized in the shear viscosity  $\eta$  (6–8). Therefore, different transport regimes are characterized by the exponent  $\beta$  of the width-dependence  $\rho \sim w^{-\beta}$ .

As shown in Fig. 1B, all ribbons investigated consistently exhibit a constant  $\rho = \rho_0$  above 150 K. In accordance with the bulk measurements (25),  $\rho$  increases linearly with increasing  $T$ , as expected for dominant electron-phonon scattering. At lower temperatures, however,  $\rho$  becomes a non-monotonic function of  $T$  and increases with decreasing  $w$ . The change of slope in  $\rho(T)$  is more pronounced in narrower ribbons, corroborating the importance of the sample's spatial boundaries in this temperature regime. Extracting the exponent  $\beta = \log(\rho)/\log(w)$  from the experimental data (Fig. S3), we found that the low temperature regime ( $T < 20$  K) is well described by an inverse quadratic relation  $\rho \sim w^{-2}$  (Fig. 1D), in agreement with the Navier-Stokes description of hydrodynamic flow (6–8). Extrapolating  $\rho(w)$  to large  $w$ , the residual resistivity of about 4 n $\Omega\text{cm}$  at 4 K matches the bulk resistivity excellently. This result allows for a quantitative extraction of the kinematic shear viscosity of the electron liquid as  $\eta = 2 \times 10^{-2} \text{ m}^2 \text{ s}^{-1}$  at 4 K (Supplementary Materials). Multiplied by the mass density  $M = nm^*$ , we obtain a dynamic viscosity of about  $\eta_{\text{D}} = 1 \times 10^{-4} \text{ kg m}^{-1} \text{ s}^{-1}$  at 4 K, which is on the order of liquid nitrogen at 75 K. While the observed  $w^{-2}$ -dependence provides strong evidence of purely hydrodynamic electron flow in  $\text{WP}_2$ , the regime between 20 K and 150 K can be explained by a smooth transition to a hybrid state, in which

viscosity-stimulated boundary scattering mixes with momentum-relaxing electron-phonon collisions (20).

Next, we investigated the Lorenz number  $L = \kappa T \rho$  in WP<sub>2</sub>, which is widely considered to be an important observable to characterize thermal and charge transport characteristics (4, 9, 23, 27). Therefore, we determined the thermal conductivity  $\kappa$  of the 2.5  $\mu\text{m}$ -wide WP<sub>2</sub> sample. The ribbon was mounted on a microsystem platform (27, 28) with two integrated heater/sensors as shown in Fig. 2A. The sensor device is thermally insulated through 1.2 mm-long silicon nitride bars operated in vacuum to  $1.6 \times 10^{-5}$  K/W at room temperature. The fabrication and characterization of the platform are described in detail in the Supplementary Materials. Two gold resistors, serving as both thermometers and heaters, were calibrated at each temperature and used to measure both, the temperature bias along and the heat flux through the WP<sub>2</sub> sample. Although used routinely for the thermal characterization of micro- and nanoscale samples, this method often suffers from thermal contact resistance effects. To minimize such effects, we chose large dimensions for the electrical contacts to the sample.

The experimentally extracted  $\kappa$  as a function of  $T$  is given in Fig. 2B. In conventional conductors, the Wiedemann-Franz law holds, i.e.  $L$  equals the Sommerfeld value  $L_0 = \pi^2 k_B^2 / (3e^2)$ . In hydrodynamic systems, however, one may expect a lowering of  $L$  due to the difference between the two relaxation times  $\tau_{\text{mr}}$  and  $\tau_{\text{er}}$ , governing electrical and thermal transport, respectively (1, 4, 9, 29). As shown in Fig. 2C, the Wiedemann-Franz relationship holds above 150 K, as the Lorenz number assumes the Sommerfeld value  $L \approx L_0$ . With decreasing temperature, however,  $L$  is strongly reduced to a value below  $0.05 L_0$  at 20 K. Hence, we expect the ratio between  $\tau_{\text{mr}}$  and  $\tau_{\text{er}}$  to be at least one order of magnitude (4). However, we note that this can only be a lower bound of the difference between the scattering times in the electron system, because of residual phonon contributions to  $\kappa$ . The observed maximum in thermal conductance at around 10 K is consistent with this notion. The Lorenz value obtained here belongs to the lowest values ever reported (27). We therefore take our observation as strong, independent indication of a purely hydrodynamic electron fluid below 20 K.

Exploiting the well-justified conjecture of the hydrodynamic nature of transport in WP<sub>2</sub> at low temperatures, we can now manipulate and tune the viscosity of the electron fluid to obtain further information on the magnitudes of  $\tau_{\text{er}}$ . For this, the resistivity of the micro-ribbons is measured as a function of the magnetic field  $\mathbf{B}$  at fixed  $T$ .  $|\mathbf{B}| = B$  is set along the  $b$ -axis of the crystal and thus perpendicular to the direction of current flow. In an electron liquid, the viscosity is defined by the internal friction between layers of different velocities (7), mediated by the exchange of electrons (Fig. 3A). The strength of the friction is given by the penetration depth  $\lambda_p$  of the electrons, which is on the order of the mean-free-path between collisions  $\lambda_p \approx l_{\text{er}}$  at zero magnetic field. When  $\mathbf{B}$  is turned on, however, this penetration depth is limited by the cyclotron radius  $r_c = mv_F/eB$ . Thus, in a strong magnetic field, the viscosity should tend to zero, providing a mechanism for a large negative magneto-resistivity. Solving the corresponding magnetohydrodynamic equations results in the magnetic-field-dependent viscosity along the  $a$ -axis of the crystal  $\eta(\mathbf{B}) = \eta_0 / (1 + (2\tau_{\text{er}}\omega_c)^2)$ , where  $\omega_c = v_F/r_c$  is the cyclotron frequency (7, 8, 30).

As shown in Fig. 3B, we observe a large negative magneto-resistivity at low temperatures. When  $\rho(\mathbf{B})$  is normalized by  $w^{-2}$ , all experimental data below 20 K collapses onto a single curve, matching the magnetic-field-dependent viscosity model excellently. The average viscosity of the single traces at zero field  $\eta_0$  equals the viscosity  $\eta$  obtained from the  $w^{-2}$ -fits above. This agreement is an

important cross-check, confirming our results and hydrodynamic interpretation. Furthermore, in accordance with the theory,  $\eta(B)$  tends to zero as the magnetic field is enhanced. The  $\tau_{\text{er}}$  extracted at individual  $T$  values are plotted in Fig. 3C. For comparison, we also extracted the timescale of the kinetic-energy dissipation related to the electrons' momentum.  $\tau_{\text{mr}}$  is extracted from Hall measurements on the bulk sample (Supplementary Materials). Throughout the entire hydrodynamic regime, we find that the intrinsic thermal energy dissipation of the electron liquid is tied to the Planckian limit (1, 11, 12) as  $\tau_{\text{er}} \sim \tau_{\hbar} = \hbar/(k_B T)$ . However, at these low temperatures,  $\tau_{\text{mr}}$  is three orders of magnitudes larger than this bound. Consequently,  $l_{\text{er}} < w \ll l_{\text{mr}}$  (Fig. S10), validating the hydrodynamic treatment of transport in WP<sub>2</sub>. As an important cross-check, we calculate the kinematic shear viscosity (7, 8) from  $\tau_{\text{er}}$  as  $\eta = v_F \tau_{\text{er}}/4$ , which gives consistent values with those extracted above (Fig. S11).

The quasi-conserved  $\tau_{\text{mr}}$  at Planckian  $\tau_{\text{er}}$  supports the recent conjecture (10) that there is a universal lower limit to the dissipation time, regardless of which and how many sources of scattering are combined. The natural question arising from this observation is therefore whether Planckian dissipation is exclusive to the hydrodynamic regime in WP<sub>2</sub>. To address this question, we perform Hall measurements on the bulk sample in the  $T$ -linear regime above 150 K (Fig. S3), where strong electron-phonon interactions yield  $L = L_0$ , because  $\tau_{\text{er}} = \tau_{\text{mr}}$ . Converting the Hall data to scattering times (Supplementary Materials) reveals that, despite their fundamental difference, electron-phonon and electron-defect processes are also tied to  $\tau_{\hbar}$  when electron-electron processes are negligible. These findings indicate that the dissipation in WP<sub>2</sub> is insensitive to the details of the scattering processes and is generally tied to a characteristic time scale  $\tau_{\hbar}$ .

In conclusion, our experiments demonstrate the existence of a hydrodynamic electron fluid in WP<sub>2</sub>. The accompanying independence of  $\tau_{\text{er}}$  and  $\tau_{\text{mr}}$  enables the isolation of the intrinsic thermal energy dissipation process, which is particularly elusive in other contexts. Remarkably, it turns out that the electron system generates entropy in a very simple and universal way, in which the only relevant scale is the temperature.

### **Acknowledgments:**

The authors thank Steffen Reith and Valentina Troncale for technical support as well as Stuart Parkin and Andrew Mackenzie for fruitful discussions. We also acknowledge support by Walter Riess and Kirsten Moselund and thank Charlotte Bollinger for copy-editing.

## References:

1. S. A. Hartnoll, Theory of universal incoherent metallic transport. *Nat Phys.* **11**, 54–61 (2015).
2. A. V. Andreev, S. A. Kivelson, B. Spivak, Hydrodynamic description of transport in strongly correlated electron systems. *Phys. Rev. Lett.* **106** (2011).
3. A. Lucas, J. Crossno, K. C. Fong, P. Kim, S. Sachdev, Transport in inhomogeneous quantum critical fluids and in the Dirac fluid in graphene. *Phys. Rev. B - Condens. Matter Mater. Phys.* **93** (2016).
4. A. Principi, G. Vignale, Violation of the Wiedemann-Franz Law in Hydrodynamic Electron Liquids. *Phys. Rev. Lett.* **115** (2015).
5. L. Levitov, G. Falkovich, Electron viscosity, current vortices and negative nonlocal resistance in graphene. *Nat Phys.* (2016).
6. R. N. Gurzhy, A. N. Kalinenko, A. I. Kopeliovich, Hydrodynamic effects in the electrical conductivity of impure metals. *Sov. Physics-JETP.* **69**, 863–870 (1989).
7. P. S. Alekseev, Negative magnetoresistance in viscous flow of two-dimensional electrons. *Phys. Rev. Lett.* **117** (2016).
8. T. Scaffidi, N. Nandi, B. Schmidt, A. P. Mackenzie, J. E. Moore, Hydrodynamic Electron Flow and Hall Viscosity. *Phys. Rev. Lett.* **118**, 226601 (2017).
9. R. Mahajan, M. Barkeshli, S. A. Hartnoll, Non-Fermi liquids and the Wiedemann-Franz law. *Phys. Rev. B - Condens. Matter Mater. Phys.* **88** (2013).
10. J. A. N. Bruin, H. Sakai, R. S. Perry, A. P. Mackenzie, Similarity of Scattering Rates in Metals Showing T-Linear Resistivity. *Science* **339**, 804–807 (2013).
11. S. Sachdev, *Quantum Phase Transitions* (2006).
12. J. Zaanen, Why the temperature is high. *Nature.* **430**, 1–2 (2004).
13. S. Sachdev, Holographic metals and the fractionalized fermi liquid. *Phys. Rev. Lett.* **105** (2010).
14. M. Cubrović, J. Zaanen, K. Schalm, String theory, quantum phase transitions, and the emergent Fermi liquid. *Science.* **325**, 439–444 (2009).
15. S. A. Hartnoll, P. K. Kovtun, M. Müller, S. Sachdev, Theory of the Nernst effect near quantum phase transitions in condensed matter and in dyonic black holes. *Phys. Rev. B - Condens. Matter Mater. Phys.* **76** (2007).
16. P. K. Kovtun, D. T. Son, A. O. Starinets, Viscosity in strongly interacting quantum field theories from black hole physics. *Phys. Rev. Lett.* **94** (2005).
17. A. Adams, L. D. Carr, T. Schäfer, P. Steinberg, J. E. Thomas, Strongly correlated quantum fluids: Ultracold quantum gases, quantum chromodynamic plasmas and holographic duality. *New J. Phys.* **14** (2012).
18. C. Cao *et al.*, Universal Quantum Viscosity in a unitary fermi Gas, *Science* **331**, 6013 (2012).

19. C. C. Homes, S. V Dordevic, M. Strongin, D. a Bonn, R. Liang, A universal scaling relation in high- temperature superconductors. *Nature*. **430**, 539–541 (2004).
20. P. J. W. Moll *et al.*, Evidence for hydrodynamic electron flow in PdCoO<sub>2</sub>. *Science*. **351**, 1061–4 (2016).
21. L. W. Molenkamp, M. J. M. De Jong, Electron-electron-scattering-induced size effects in a two-dimensional wire. *Phys. Rev. B*. **49**, 5038–5041 (1994).
22. D. A. Bandurin *et al.*, Negative local resistance caused by viscous electron backflow in graphene. *Science*. **351**, 1055–1058 (2016).
23. J. Crossno *et al.*, Observation of the Dirac fluid and the breakdown of the Wiedemann-Franz law in graphene. *Science*. (2016) (available at <http://science.sciencemag.org/content/early/2016/02/10/science.aad0343.abstract>).
24. R. K. Kumar *et al.* , Super-ballistic flow of viscous electron fluid through graphene constrictions. *arXiv:1703.06672*.
25. N. Kumar *et al.* , Extremely high magnetoresistance and conductivity in the type-II Weyl semimetal WP2. *arXiv:1703.04527* (2017).
26. H. Takatsu *et al.*, Extremely large magnetoresistance in the nonmagnetic metal PdCoO 2. *Phys. Rev. Lett.* **111** (2013).
27. S. Lee *et al.*, Anomalously low electronic thermal conductivity in metallic vanadium dioxide. *Science*. **355**, 371–374 (2017).
28. S. F. Karg *et al.*, Full thermoelectric characterization of InAs nanowires using MEMS heater/sensors. *Nanotechnology*. **25**, 305702 (2014).
29. M. A. Tanatar, J. Paglione, C. Petrovic, L. Taillefer, Anisotropic Violation of the Wiedemann-Franz Law at a Quantum Critical Point. *Science*. **316**, 1320–1322 (2007).
30. M. S. Steinberg, Viscosity of the electron gas in metals. *Phys. Rev.* **109**, 1486–1492 (1958).

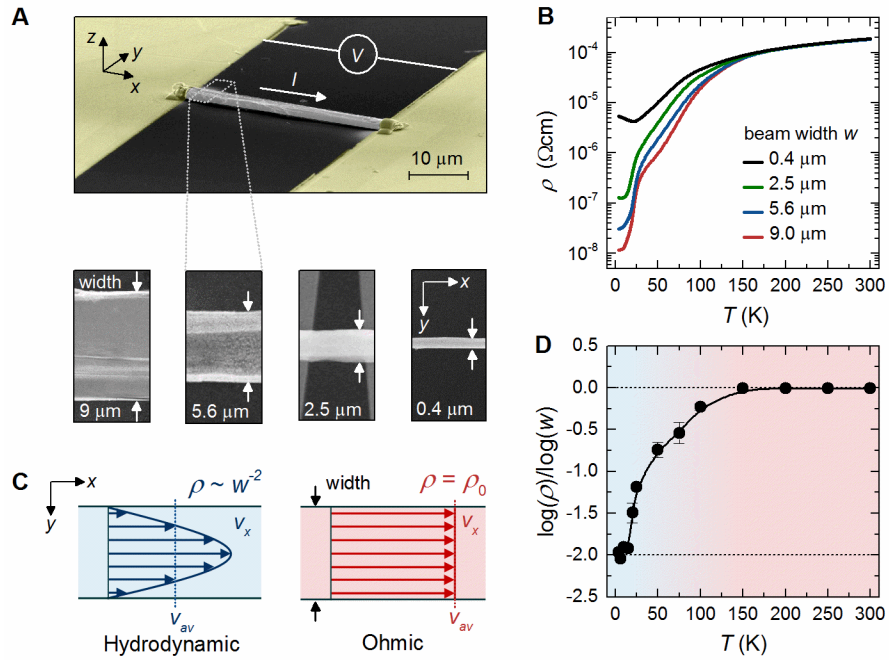


**Fig. 1. Effect of the channel width on the electrical resistivity.** (A) False-colored scanning electron beam microscopy (SEM) image of the device to measure the electrical resistance  $R = V/I$  (upper panel) of the  $\text{WP}_2$  micro-ribbons. Beams of four different widths  $w$  were investigated (lower panels). (B) Temperature-dependent electrical resistivity  $\rho$  of the four beams. (C) Sketch of the velocity  $v_x$  flow profile for a Stokes flow (left panel) and conventional charge flow (right panel).  $v_{\text{av}}$  is the average velocity of the charge carrier system. (D) Exponent of the functional dependence  $\rho(w)$  as a function of temperature, extracted from the data plotted in (A). The colored background marks the hydrodynamic (light blue) and the normal metallic temperature regime (light red).

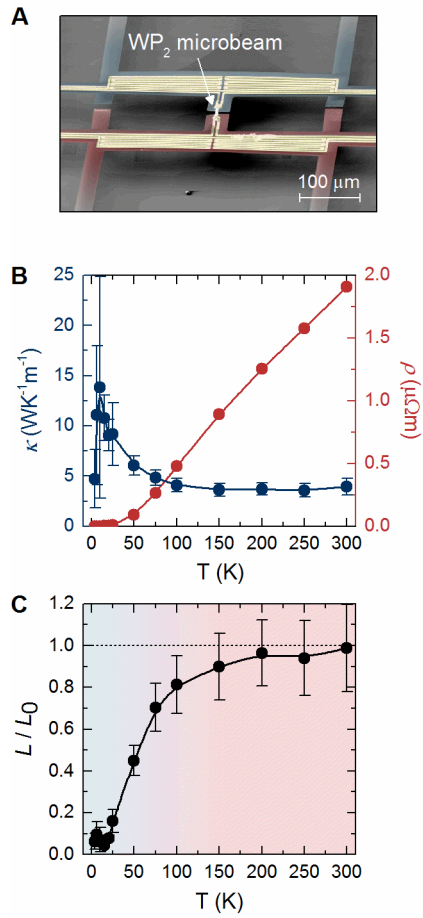


**Fig. 2. Violation of the Wiedemann-Franz law.** (A) False-colored SEM image of a microdevice for measuring thermal transport that consist of two suspended platforms that are bridged by the 2.5 μm-wide WP<sub>2</sub> ribbon. (B) Thermal conductivity  $\kappa$  (left axis) and electrical resistivity (right axis)  $\rho$  of the micro-ribbon as a function of temperature. (C) Lorenz number  $L = \kappa T \rho$ , calculated from the data in (B).

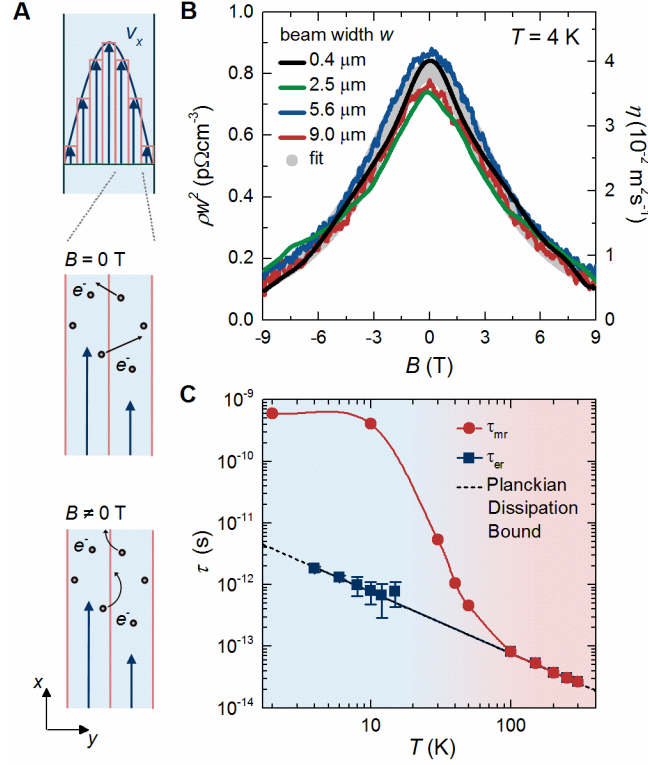


**Figure 3. Magneto hydrodynamics and Planckian bound of dissipation.** (A) The origin of the decrease of the electron viscosity  $\eta$  in a magnetic field  $B$  (schematic). The viscous friction between two adjacent layers of the electron fluid moving with different velocities is determined by the depth of the interlayer penetration of the charge carriers  $e^-$ . In a magnetic field, this depth is limited by the cyclotron radius. (B)  $\rho$  as a function of  $B$  for all four WP<sub>2</sub> beams investigated at 4 K, normalized by their width  $w$  (lines). The experimental data has been fitted by the magneto hydrodynamic model in the Navier-Stokes flow limit (grey dots). (C) Experimentally extracted momentum and thermal energy relaxation times  $\tau_{mr}$  and  $\tau_{er}$ , respectively (symbols with guide to the eyes). The dashed line marks the Planckian bound on the dissipation time  $\tau_{\hbar} = \hbar/(k_B T)$ .